Transition Metal Chemistry
https://doi.org/10.1007/s11243-024-00608-4

Optimized green synthesis of biocompatible Ag nanostructures using *Artemisia Indica* leaf extract: a promising avenue for biomedical applications

Manoj Manikrao Gadewar[1] · G. K Prashanth[2] · Srilatha Rao[3] · H. S. Lalithamba[4] · N. P. Bhagya[5] · A. S. Sowmyashree[3] · K. Shwetha[3] · Hemantkumar N. Akolkar[6]

Received: 14 June 2024 / Accepted: 7 September 2024

Abstract

Artemisia indica, belonging to the family Asteraceae, is renowned for its rich phytoconstituents and traditional medicinal uses. This study aimed to optimize the green synthesis of biocompatible Ag NPs using varying concentrations of *A. indica* leaf extract and AgNO3. The objectives were to characterize the synthesized NPs and evaluate their potential biomedical applications. The synthesized NPs were characterized using FTIR, XRD, TEM, and Zeta sizer. The results indicated an average particle size of approximately 20 nm and a zeta potential of −23.4 mV, confirming their stability. PXRD analysis demonstrated the crystalline nature of the NPs, while FTIR analysis confirmed the capping of phytoconstituents on the nanoparticle surface. Biocompatibility was assessed using the MTT assay on the L929 cell line, showing 83% cell viability, indicating non-toxicity. Additionally, the green-synthesized NPs exhibited significant antibacterial activity at a concentration of 500 µg/mL, as evidenced by a clear zone of inhibition. This study highlights a rapid, eco-friendly synthesis method for Ag NPs, paving the way for novel biomedical applications.

Abbreviations

A. indica	*Artemisia indica*
Ag	Silver
NPs	Nanoparticles
$AgNO_3$	Silver nitrate
Ag-AI-NPs	Silver-*Artemisia indica* nanoparticles
UV	Ultraviolet
DMEM	Dulbecco's modified eagle medium
DPPH	1, 1-Diphenyl-2-picrylhydrazyl
CH_3OH	Methanol
FBS	Fetal bovine serum
FTIR	Fourier transform infrared
ZOI	Zone of inhibition
MLE	Methanolic leaf extract
MTT	(3-[4, 5-Dimethylthiazole-2-yl]-2, 5-diphenyl tetrazolium bromide)
PBS	Phosphate-buffered saline
SPR	Surface plasmon resonance
TEM	Transmission electron microscopy
PXRD	Powder X-ray diffraction
ZP	Zeta potential
PS	Particle size
DLS	Dynamic light scattering
TGA	Thermo-gravimetric analysis
DSC	Differential scanning calorimetry
SAED	Selected area electron diffraction
E. coli	*Escherichia coli*
P. aeruginosa	*Pseudomonas aeruginosa*

✉ G. K Prashanth
prashanth_chem@sirmvit.edu

[1] Department of Pharmacology, School of Medical and Allied Sciences, KR Mangalam University, Gurgaon 122 103, India

[2] Department of Chemistry, Research and Development Centre, Sir M. Visvesvaraya Institute of Technology, Bengaluru 562 157, India

[3] Department of Chemistry, Nitte Meenakshi Institute of Technology, Bengaluru 560 064, India

[4] Department of Chemistry, Siddaganga Institute of Technology, Tumkur 572 103, India

[5] Department of Chemistry, Sai Vidya Institute of Technology, Bengaluru 560 064, India

[6] Department of Chemistry, Abasaheb Marathe Arts, and New Commerce, Science College, Ratnagiri 416 702, India

Published online: 18 September 2024

Introduction

Green synthesis methods for NPs have gained significant attention due to their eco-friendliness and potential biomedical applications. Zinc oxide NPs synthesized using Nostoc sp. demonstrated antioxidant and antimicrobial properties [1], while iron oxide NPs from *Leptolyngbya* sp. L-2 showed promising pharmacogenetic properties for drug delivery and cancer therapy [2]. Silver oxide NPs from *Nodularia haraviana* revealed significant antimicrobial properties [3], and Anabaena sp. A-1-mediated molybdenum oxide NPs exhibited excellent antibacterial and antifungal activities [4]. ZnO NPs using *Piper betle* leaf extract induced apoptosis in breast cancer cells [5], and Ag/CuO nanocomposites showed antimycobacterial, antioxidant, and anticancer activities [6]. ZnO NPs from solution combustion synthesis using lemon juice exhibited notable antitubercular activity [7], and ZnO NPs from combustion-assisted green methods displayed effective antibacterial and cytotoxic properties [8].

Nanotechnology is extensively used in biomedical sciences [9], focusing on alternative drug delivery systems with metal oxides like gold [10], zinc [11], copper [12], silver [13, 14], and titanium dioxide [15]. Ag-NPs offer advantages like bacterial cell penetration and high surface area-to-volume ratio, working through silver ion release, reactive oxygen species generation, cell membrane permeation, and DNA replication blockage [16], with no reported ingestion toxicity [17].

Various methods impact Ag-NPs yield and efficacy. Top-down approaches include laser ablation [18], mechanical milling [19], electroblasting, and etching [20]. Bottom-up approaches include the sol–gel process [21], supercritical fluid [22], laser pyrolysis [23], chemical reduction [24], and green synthesis [25–27]. Green synthesis, using plant extracts, is favored for its biocompatibility, eco-friendliness, cost-effectiveness, and scalability [28], with plant constituents acting as reducing agents [29].

Biofabricated NPs show significant promise for biomedical applications. Ag NPs synthesized using *Lagerstroemia speciosa* induce apoptosis in osteosarcoma cells (MG-63) [30], while *Cardamine hirsuta* leaf extract-mediated NPs exhibit anticancer potential against the Caco-2 cell line [31]. Zinc oxide NPs from *Talaromyces islandicus* show antibacterial, anti-inflammatory, bio-pesticidal, and seed growth-promoting activities [32]. Ag NPs from *Ixora brachypoda* exhibit strong antimicrobial activity [33], and those from Plumeria alba show antimicrobial effects and anti-oncogenic activity against glioblastoma cells (U118 MG) [34]. *Catharanthus roseus*-synthesized NPs modulate inflammatory responses and have anti-oncogenic potential [35].

Artemisia L., an abundant genus in the Asteraceae family, is used in folk medicine for various ailments [36]. *A. indica*, known as "Titepati" in Darjeeling and Indian wormwood in India [37], is used to treat asthma, amoebic dysentery, and other conditions [36]. It contains antimalarial compounds like maackiain and artemisinin [38, 39] and has anti-inflammatory properties reported in lung, breast, colon, and breast cancer [40]. Compounds from *A. indica* show antiepileptic and antidepressant activities [41], and it is used as an anti-diabetic, anti-inflammatory, and anthelminthic agent [37, 42–44]. Green synthesis using various bio-systems is favored for its ease of use and plant diversity [17, 45–52].

In this study, given the widespread use of *A. indica*, we synthesized Ag NPs using the green leaf extract of *A. indica*. The NPs were characterized by FTIR, XRD, and TEM to confirm their size. The in vitro antibacterial and cytotoxic activities of Ag-AI-NPs were evaluated. This study reports the rapid and easy synthesis of stable Ag NPs with significant antibacterial activity, focusing on green synthesis using *A. indica* leaf extract, characterization, and evaluation of antibacterial and cytotoxicity properties.

Materials and methods

Chemicals

Silver nitrate ($AgNO_3$), 2,2-diphenyl-1-picrylhydrazyl (DPPH), methanol (CH_3OH), ascorbic acid, 3-(4,5-dimethylthiazol-2-yl)-2,5-diphenyl tetrazolium bromide (MTT), dimethyl sulfoxide (DMSO), phosphate buffer saline (PBS), Dulbecco's modified eagle medium (DMEM), and fetal bovine serum (FBS) of analytical purity were purchased from Sigma-Aldrich. The plant collection was done from Nagaland local market and authenticated.

Collection of leaves and preparation of plant extract

Fresh leaves of the plant *A. indica* were collected between July and September from the village of Kohima District of Nagaland. The leaf of the plant was authenticated by Curator, Department of Botany, Guwahati University, Assam. The herbarium was prepared and voucher specimen sample (18,380) was deposited for future reference. The leaves were washed thrice with water and dried in shade at room temperature for 15 days. In addition, the leaves were ground into a fine powder using an electric mixer (Bajaj GX 11). About 100 g of powder from the plant was extracted using 250 mL of methanol. The solution weas kept at room temperature at constant pressure for one week, after which filtered with Whatman No. 1 filter paper. The filtrate was vacuumed and the extract was stored at 4 °C for further experiments.

Antioxidant assay

Antioxidant activity of extract was measured by DPPH scavenging assay by using gallic acid as a standard followed by experimental analysis for the presence of various phytoconstituents like phenolic and flavonoids compounds was performed as per the protocol Sánchez-Moreno et al. and chang et al., respectively [53, 54]. The solution of DPPH was prepared and it was kept in dark room for 24 h. The stock solution of extract was prepared by dissolving 5 mg of extract in 5 mL of methanol (1 mg/mL). Various concentrations of solutions have been prepared ranging from 5 to 100 µg/mL from stock solution and they were combined with 0.1 mM methanolic solution of DPPH. This solution was incubated for 30 min at room temperature and was recorded at 517 nm.

The percentage radical scavenging activity of extract was calculated using formula.

$$\%\ \text{Anti} - \text{oxidant activity} = \text{Absorbance of control} - \text{Absorbance of sample} / \text{Absorbance of sample} \times 100$$

Green synthesis and optimization of Ag-AI-NPs

Green synthesis of colloidal Ag-AI-NPs was achieved using (0.1 M) aqueous solution of $AgNO_3$. MLE in the concentrations range of 1–10% (v/v) taken as a reducing agent were allowed to react with $AgNO_3$ solution at room temperature. 5% (v/v) of the MLE of the plant was optimized concentration selected for further studies. About 1.25 mg/mL methanolic extract of the plant was mixed with 0.1 M aqueous $AgNO_3$ solution in different volume ratios (0.5:9.5 to 9.5:0.5) according to standard protocols [55, 56]. The mixtures were exposed to sunlight for about 15 min to observe the color change. This was followed by incubating the mixtures for 24 h and exposed to sunlight for the conversion of Ag^+ ions to Ag^0 and promote maximum formation of Ag-AI-NPs. It was mixed thoroughly and placed in the microwave oven (Samsung, Model MC32A7035) for the process of reduction into Ag-AI-NPs and observed for color change [57]. The optimized reaction time was 120 s at a temperature of 100–120 °C. All reactions were done in triplicate.

Characterization

The biosynthesized Ag-AI-NPs were characterized using various physical methods, consistent with the techniques employed in previous studies [58–61].

UV–vis analysis

Green synthesized Ag-AI-NPs were characterized by using Tecan Multimode Microplate Reader (Infinite M200). The green synthesized Ag-AI-NPs were dispersed in an appropriate solvent, typically water or an ethanol–water mixture, to form a colloidal solution. The dispersion should be clear and free of aggregates to ensure accurate measurements. The prepared colloidal solution was placed in a well of the Infinite M200. The instrument scans across a range of wavelengths, typically from 200 to 800 nm, to record the absorbance spectrum. The UV–Vis spectrum is used to determine the surface plasmon resonance (SPR) peak, which provides information about the size, shape, and distribution of the NPs.

The surface plasmonic resonance (SPR) of Ag-AI-NPs was recorded by measuring the absorbance at 300 nm–700 nm to indicate the typical peak of Ag which further indicates the reduction of Ag ions.

Particle size and zeta potential

Particle size and zeta potential of the Ag-AI-NPs were determined by Nano Zeta sizer (Malvern, UK). The Ag-AI-NPs are dispersed in an appropriate solvent, usually water, to form a homogenous colloidal solution. The concentration should be optimized to avoid multiple scattering effects but still be sufficient for accurate measurements.

Particle size of the NPs was determined by dilution method. The prepared colloidal solution was placed in a cuvette or specialized sample holder for the Nano Zeta sizer (Malvern, UK). DLS is used to measure the Brownian motion of the NPs, and the instrument calculates the hydrodynamic diameter based on the scattering data. The same colloidal solution was used to measure the zeta potential, which involves applying an electric field to the sample and measuring the velocity of the particles. This velocity is used to calculate the zeta potential, which indicates the surface charge and stability of the NPs in the suspension. The sample was diluted by double distilled water up to 10 times. A disposable cuvette was filled with 1 mL of the diluted sample and tested at 25 °C at 90° angle. A helium–neon laser was used as a source of light and the Particle Size was determined by the particle diffusion by Brownian motion. The ZP of NPs was determined by taking it in a disposable capillary [62].

TEM

The shape and size of the prepared Ag-AI-NPs were determined by JEM-2100, 200 kV, Joel, TEM system. The sample was subjected to centrifugation for 30 min at 15,000 rpm. Further, the sample was re-suspended in 10 mL distilled water and it was stored for 24 h at 20 °C. The process of

lyophilization was done for the resultant sample. The lyophilized sample was dissolved in double distilled water and few drops were placed on copper grid. The remaining water was evaporated using hot air oven (60 °C for 3 h) [63].

PXRD

As a primary characterization tool used for measuring critical features like crystal structure and crystallite size XRD patterns have been widely used in nanoparticle research. The randomly oriented crystals in nanocrystalline materials cause broadening of diffraction peaks. This has been attributed to the absence of total constructive and destructive interferences of x-rays in a finite sized lattice. Moreover, inhomogeneous lattice strain and structural faults lead to broadening of peaks in the diffraction patterns. The size calculated from x-ray diffraction peak broadening is a measure of the smallest unfaulted regions or coherently scattering domains of the material. In fact, this is the size of regions bounded by defects and grain boundaries and separated from surrounding by a small mis-orientation, typically one or two degrees.

PXRD instrument with Bruker make (Advance D8 model) was used to record the crystallinity of formed Ag-AI-NPs. NPs were ground into a fine powder to ensure homogeneity. The powdered sample is then evenly spread onto a sample holder, often made of glass or silicon, ensuring a flat and smooth surface for accurate measurement. In thin film mode, the same was analyzed by the PXRD instrument with a Cu source at 1.5406 Å wavelength [63]. The prepared sample holder was placed in the Bruker Advance D8 model PXRD instrument. The instrument generated X-rays that were directed at the sample, where they diffracted according to the crystalline structure of the NPs. The diffracted X-rays were detected, and the resulting diffraction pattern was recorded. The PXRD pattern, which consisted of peaks corresponding to different crystal planes, was analyzed to determine the phase composition, crystallite size, and structural properties of the NPs. The positions and intensities of the peaks provided detailed information about the crystal structure and any impurities or secondary phases present in the sample.

FTIR

The Ag-AI-NPs were mixed with potassium bromide (KBr) powder and pressed into a pellet, or a drop of their dispersion was placed on an ATR crystal and dried. SHIMADZU, IR Affinity-1 was used to record the FTIR spectrum in the wave number ranging from 600 to 400 cm^{-1} with a resolution of 2 cm. 1 mg of NPs was dissolved in Milli Q water and sample was placed in liquid cell followed by recording of spectra [64]. The instrument passed an infrared beam through the sample, and the resulting spectrum displayed absorption bands corresponding to the functional groups on the NPs' surface, revealing their chemical composition.

TGA

TGA spectrum of synthesized Ag-AI-NPs was recorded on simultaneous thermal system (Shimadzu, DTG-60) in temperature range from room temperature to 900 °C. the sample was kept in platinum crucible and measurements were carried out in inert atmosphere at the heating rate of 10 °C/min. The sample pan was loaded into the instrument. The instrument heated the sample from room temperature to 900 °C at a controlled rate. The TGA spectrum recorded the weight change of the sample as a function of temperature, providing information on the thermal stability, composition, and any decomposition or oxidation processes occurring in the Ag-AI-NPs NPs.

Antibacterial activity

The Ag-AI-NPs formulated with green synthesis method were investigated for the antibacterial activity against *E. coli* (ATCC 423 strain) gram negative bacteria by using microtiter plate assay. The study was conducted at various concentrations of Ag-AI-NPs of *A. indica*. Muller Hinton agar plates were taken and they have been inoculated with fresh cultures of *P. aeruginosa* and *E. coli* (100 µL) by using sterile swabs. About 5 mm diameter wells were made on the surface of agar medium by the use of sterile gel borer. The formulated Ag-AI-NPs (about 100 µL) in 50, 150, 250 and 500 µg/mL concentrations have been poured into the formed wells and the plates were incubated for 24 h at 37 °C. ZOI was determined for all the concentrations which was finally used to determine the antibacterial activity. Ciprofloxacin and sterile water served as the positive and negative controls respectively. The average of three replications was recorded [65].

Cytotoxicity

Cytotoxicity cell assay was mainly used to detect the metabolic activity of the cells based on reduction of yellowish MTT dye to dark blue formazan by viable and metabolically active cell. The normal fibroblast cells (L929) were cultured in DMEM medium supplemented with 5% CO_2 at 37 °C with humidity of 75%. DMEM media was used to seed the confluent cells at a density of 1×10^4 in a 96-well plate made by Cell Bind, Corning Inc., Corning, NY, USA.

After 24 h of incubation, the medium was removed, and cells were then exposed to various concentrations of green synthesized silver NPs (10 to 500 µg/mL). Following a 24 h treatment period, the media was removed, 100 µL of MTT (0.5 mg/mL) was added to each well, and the wells were then

incubated at 37 °C for 4 h. After the incubation period, the media was removed, 100 µL of dimethyl sulfoxide (DMSO) was added to each well to dissolve the formazan crystals, and the absorbance was measured at 570 nm using a multiwell plate reader (Tecan micro plate reader, model 680, Tecan Inc., San Clemente, CA, USA). The percentage of cell viability was then calculated using the formula:

$$(\text{Absorbance of test solution/Absorbance of control}) \times 100. \quad (2)$$

Results and discussion

DPPH radical scavenging assay

Figure 1 depicts the Antioxidant activity of *A. indica* extract presented as percentage of DPPH radical inhibition. The extract demonstrated dose-dependent radical scavenging activity in the DPPH experiment at doses ranging from 5 to 100 µg/mL, with a maximal activity of 88.36% at that dosage (Table 1). The IC_{50} was discovered to be 83.26 µg/mL. This clearly depicts the presence of reducing phytochemicals in the extract which reduced the silver ions into the corresponding NPs.

Synthesis of Ag-AI-NPs

Figure 2 shows images of change in color of reaction mixture (Plant extract and $AgNO_3$) at different time interval from very pale yellow (0 s) to yellow–brown (120 s) indicating clearly the reduction of cationic silver to its metallic counterpart and synthesis of Ag-NPs. Reaction mixture has shown formation of stable colloidal NPs as aggregates or precipitates were not observed.

Table 1 DPPH assay of *A. indica* extract

Concentration of plant extract (µg/mL)	DPPH scavenging activity (%)
5	26.39
10	42.19
20	73.66
40	81.72
50	83.26
100	88.36

Characterization

UV- visible spectra analysis

UV–visible spectra revealed that the excitation of Surface Plasma Resonance (SPR) of synthesized Ag-AI-NPs was in the range of 400–430 nm. The SPR peaks at low concentrations of MLE of 1–3% (v/v) and very higher concentrations of 9–10% (v/v) were broad, indicating that at very high and low concentrations the NPs formation is anisotropic (Fig. 3a). The formation of Ag-AI-NPs from the plant extract was observed in a logarithmic progression. It was observed that intensity of peaks increased with increase in concentration of MLE, peaks were less sharp at lower concentration indicating MLE concentration is insufficient to reduce Ag to Ag-AI-NPs and with excess of MLE Ag becomes insufficient indicating optimum concentration is required to obtain Ag-AI-NPs. Very less change in λ_{max} (around 420 nm) was observed when the concentration of MLE increases from 1 to 10% which might be due to similarity of size and shapes of the Ag-AI-NPs present in different samples of MLE concentrations. All samples remained colloidally stable without formation of any precipitate over a period of 30 days.

Figure 3b shows SPR of Ag-AI-NPs synthesized at different time intervals (0–150 s) with 5% concentrations of

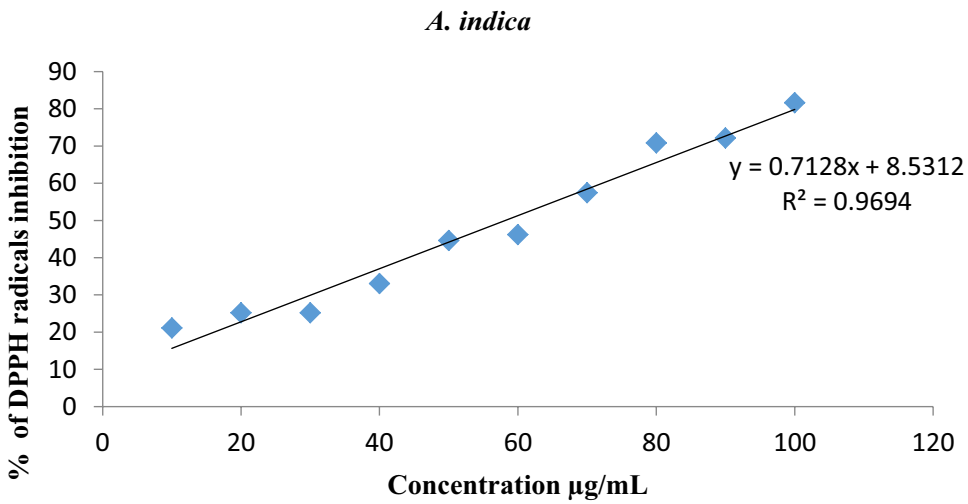

Fig. 1 Antioxidant activity of *A. indica* extract presented as percentage of DPPH radical inhibition

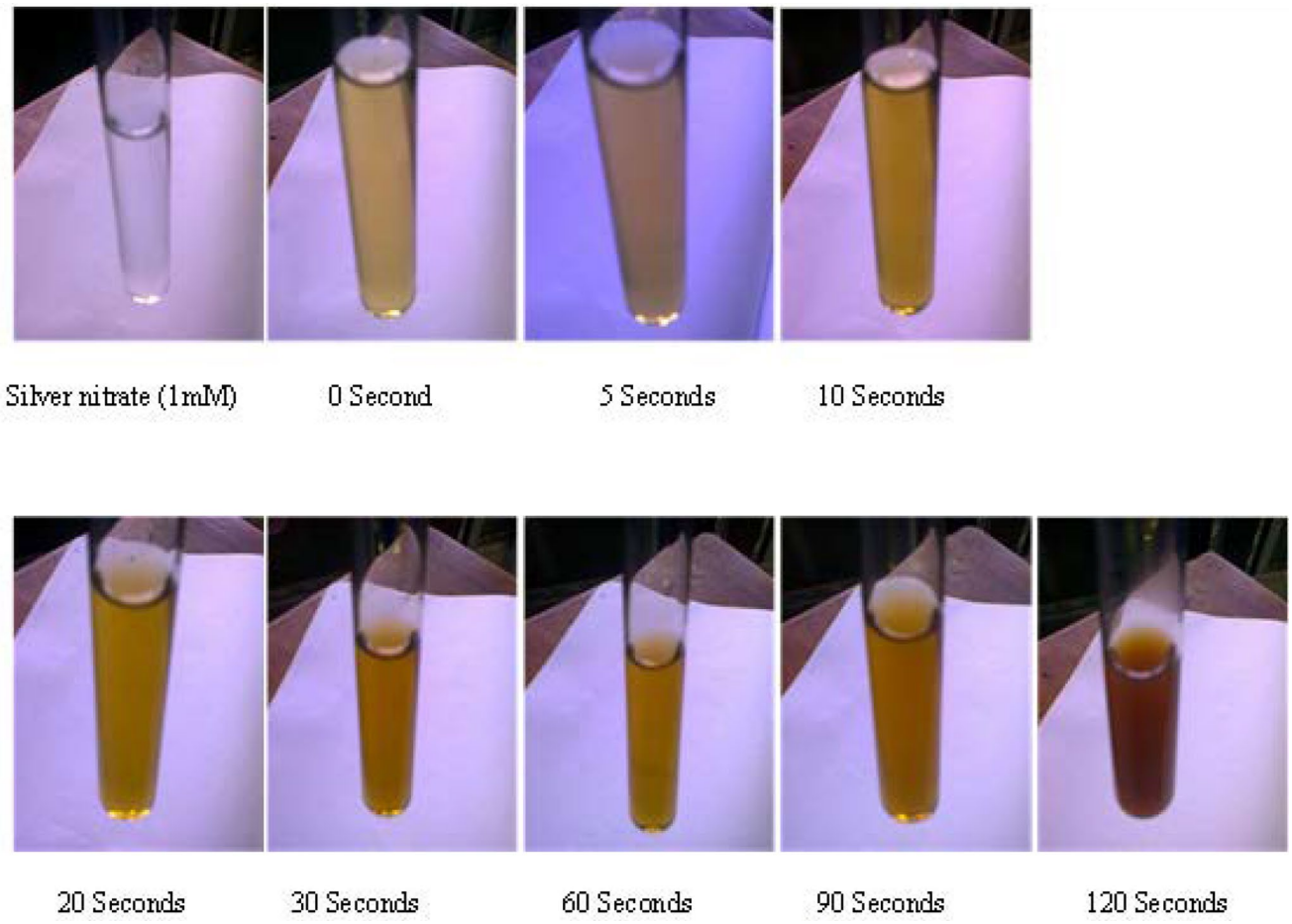

Fig. 2 Color change with time during the formation of Ag-AI-NPs

leaf extract against 1 mM $AgNO_3$ in microwave oven. It was found that on heating the solution with time (90–120 s) the SPR showed sharper peak as compared to less heating time and synthesis reaction time for Ag-AI-NPs was found to be 90 s.

Particle size and zeta potential

The particle size and zeta potential of Ag-AI-NPs were determined by Nano Zeta sizer (Malvern, UK). Laser doppler electrophoresis and DLS techniques were used to determine the same. The average particle size of the sample was found to be 20 nm (Fig. 3C and D) which was narrow size distribution range. The zeta potential of the sample was found to be −23 mV which indicated the stability of formed Ag-AI-NPs without agglomeration. High positive or negative zeta potentials greater than 30 mV depicts monodispersity while lower values can lead to agglomeration. Zeta potential is affected not only by the properties of NPs, but also the nature of the solution, such as pH and ionic strength [66].

TEM

The TEM studies of Ag-AI-NPs exhibited morphology of the particles being spherical and oval in morphology with a mean particle size of ± 20 nm. (Fig. 4a and b). UHRTEM was used to observe the Ag-AI-NPs at the atomic level and its image revealed clear lattice fringes on the particle surface (Fig. 4c) which is in accordance with the silver metal. The SAED pattern confirmed the crystalline nature of Ag-AI-NPs (Fig. 4d). 4 € depicts the histogram of the particle size distribution.

PXRD

PXRD spectrum for purified samples of Ag-AI-NPs showed four Bragg reflections depicting the face-centered cubic (FCC) structure of the synthesized NPs. The PXRD pattern presented in Fig. 5 shows the characteristic 2θ peaks at 38.1°, 44.4°, 64.8°, and 78° for Ag-AI-NPs, corresponding to the (111), (200), (220), and (311) planes of the FCC structure of metallic Ag.

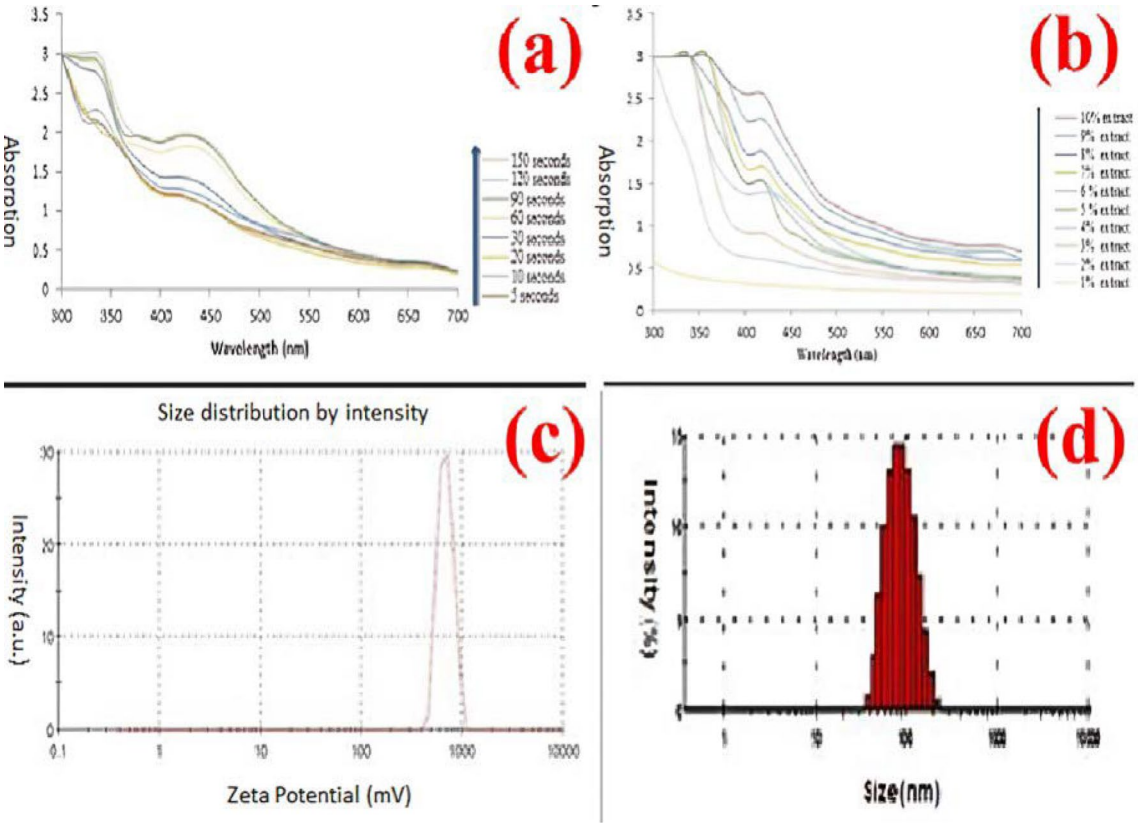

Fig. 3 **a** UV–visible absorption spectra of Ag-AI-NPs synthesized with different concentrations of MLE (1–10%) against 1 mM $AgNO_3$, **b** UV–visible absorption spectra of Ag-AI-NPs synthesized at different time intervals (0–150 s) with 5% concentrations of leaf extract against 1 mM $AgNO_3$ at room temperature, **c** Dynamic laser scattering detection of particle size distribution, **d** Particle size distribution of NPs

FTIR study

Figure 6 shows the FTIR bands for the extract and NPs showed strong bands at ~ 3394.72, ~ 1654.92; and ~ 3390.86, ~ 1656.35. The strong IR bands at ~ 3394.72 is characteristic of O–H stretching indicating phenolic type of compounds present in the extract responsible for capping. The reduction of Ag^+ ions to Ag-AI-NPs was brought about by the phytoconstituents present in MLE, and this was further confirmed by the capping of the phytochemicals onto the surface of the Ag-AI-NPs as evident from the FTIR [67].

TGA

TG-differential thermal analysis (DTA) curve of Ag-AI-NPs is presented in Fig. 7. From that it was observed that dominant loss of the sample occurred in temperature region between 250 and 500 °C. There was almost no weight loss below 500 °C that may be due to either evaporation of water and organic components. Overall, TGA results showed a loss of 60% up to 500 °C. Differential thermal analysis plot displayed an intense exothermic peak between 300 and 500 °C which mainly attributed to crystallization of silver NPs which depicts that complete thermal decomposition and crystallization of the sample occurred simultaneously**.**

Antibacterial activity

Figure 8a and b shows antibacterial activity of Ag-AI-NPs against *P. aeruginosa* (MTCC-2448) and *E. coli* (MTCC-443). Agar well diffusion assay was performed and Ag-AI-NPs with concentration of 500 µg/mL was found to exhibit a significant inhibitory effect. The clear zones of inhibition of the samples are presented in Table 2, suggesting antimicrobial activity of synthesized Ag-AI-NPs. This antibacterial effect was attributed to the diffusion of green-synthesized Ag-AI-NPs through bacterial cell wall causing physical damage to the bacterial cell and may be due to formation of reactive oxygen species. Species along with damage to the respiratory system due to leakage of cellular proteins [68].

Figure 8a–b depicts the antibacterial activity of Ag-AI-NPs against *P. aeruginosa* (MTCC-2448) *E. coli* (MTCC-443) was performed using agar well diffusion assay. At a

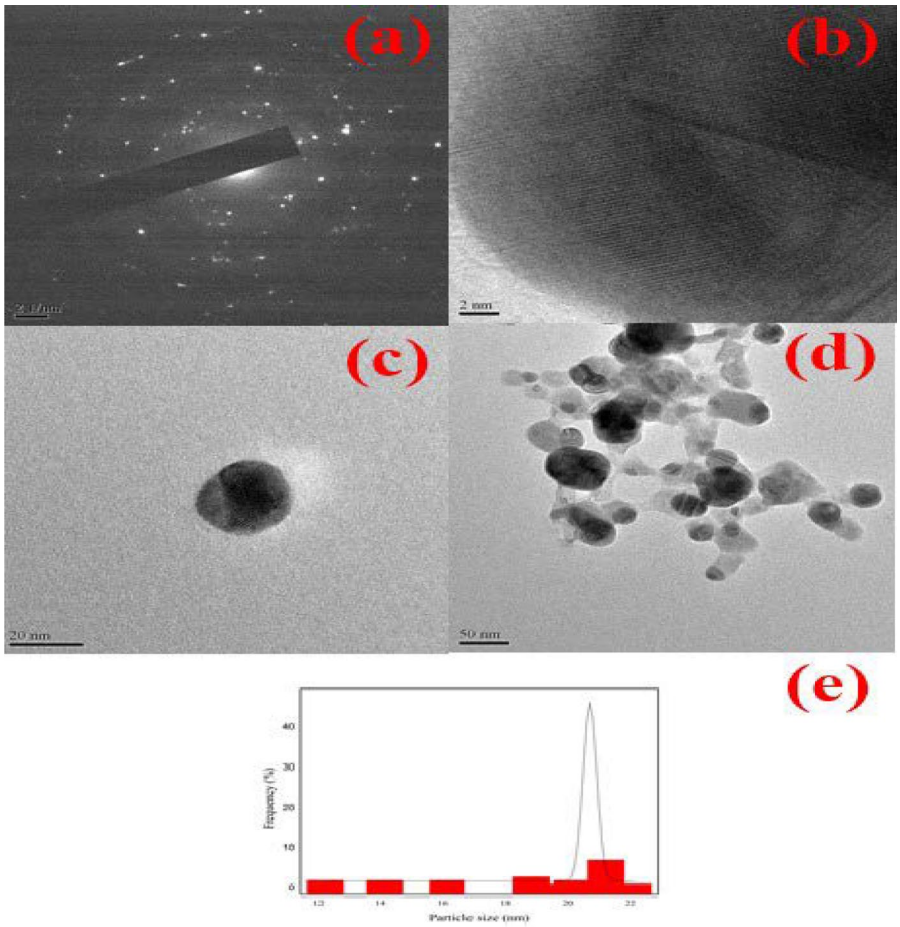

Fig. 4 **a** SAED pattern **b** HRTEM **c** and **d** TEM of Ag-AI-NPs synthesized at optimum concentration (5% MLE) **e** Histogram of particle size distribution (Particle size distribution histogram determined from the TEM images. The histogram illustrated number of particles that were in the field of view of the transmission electron microscope. Total number of NPs was 293 with particle size of 20 nm)

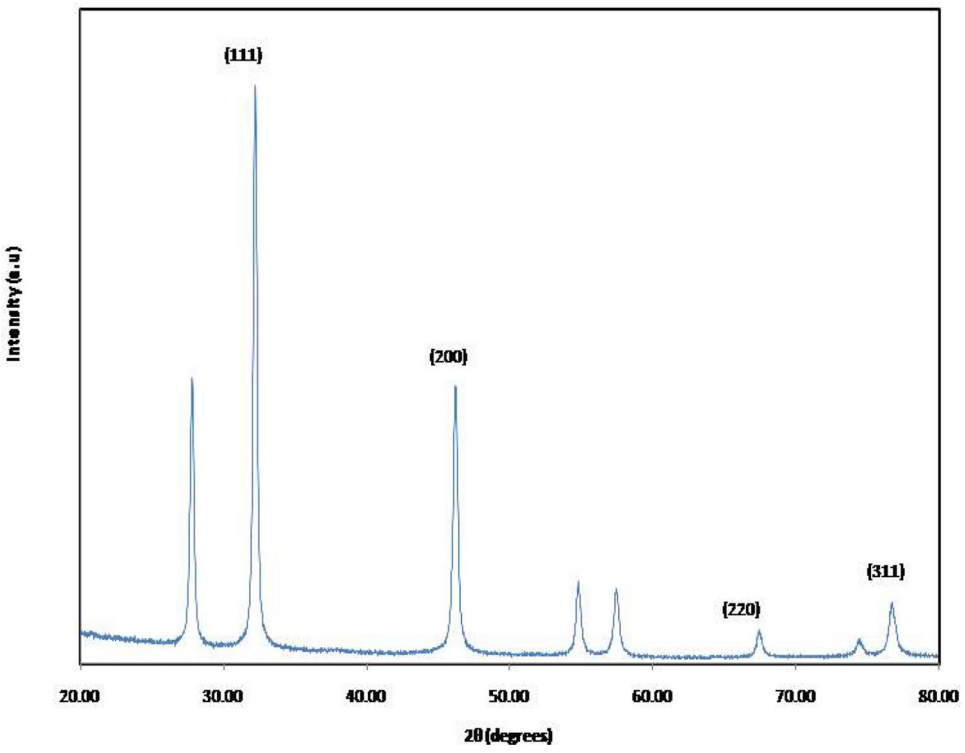

Fig. 5 XRD analysis of Ag-AI-NPs

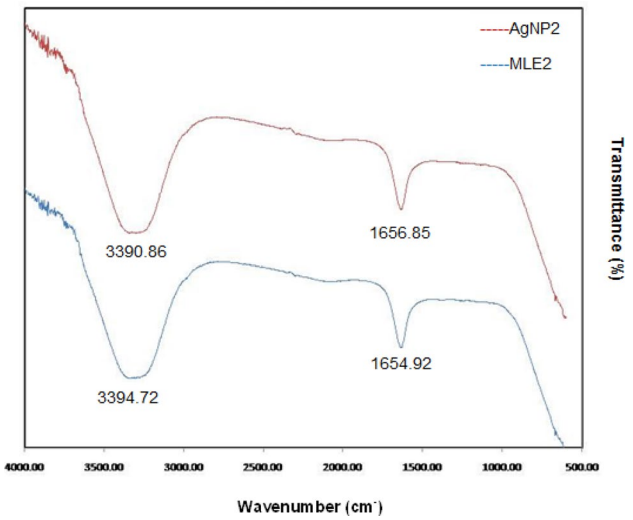

Fig. 6 FTIR analysis of Ag-AI-NPs

concentration of 1 µg/mL, the sample exhibited a significant inhibitory effect as presented in Table 2 and Fig. 8.

Statistical analysis of the data was carried out by two-way ANOVA using Graphpad prism 5.0 (Graph Pad Software Inc., San Diego, USA) as presented in Fig. 9. P-values 0.05 were assumed to be significant. Ag-AI-NPs showed significant ($p < 0.05$) cytotoxicity. The activity was found to be significant at a concentration of 1 mg/mL of NPs.

Cytotoxicity and cell viability

Cytotoxicity studies were carried out using normal fibroblast cell (L929) to confirm safety and biocompatibility of green-synthesized Ag-AI-NPs. Normal fibroblast cell (L929) treated with different concentrations of Ag-AI-NPs for 24 h showed 83% cell viability at highest concentration of (500 µg/mL) (Fig. 10) indicating biocompatibility of synthesized Ag-AI-NPs and can be used for various biomedical applications. Treatment of L929 cell line with different concentration of ampicillin-treated $AgNO_3$ showed concentration-dependent cell viability and showed 78% of cell viability at highest concentration of (500 µg/mL) as shown in Fig. 11 which is close to the % cell viability shown by green-synthesized Ag-AI-NPs.

The mechanism by which Ag NPs exhibit cytotoxicity involves the generation of reactive oxygen species (ROS) and the formation of superoxide anions ($*O_2^-$), as evidenced by recent studies [69, 70]. The release of silver ions from the NPs leads to the induction of cancer cell death. Therefore, the solution combustion-synthesized Ag-AI-NP's cytotoxicity on L929 cells can be attributed to these silver ions [13]. This effect is dose-dependent, varying with concentration and differing in impact between normal and cancerous cells [64, 65].

Figure 12 illustrates optical microscopic images depicting the effects of Ag-AI-NPs and $AgNO_3$ treatment on L929 cells.

Conclusion

Biocompatible and eco-friendly plant-mediated Ag NPs of vary small diameter of 20 nm were synthesized using *A. Indica.* UV studies affirmed the formation of Ag NPs and TEM confirmed the formation spherical NPs. PXRD revealed the crystalline nature of NPs, whereas FTIR supported the presence of phytoconstituents on the surface

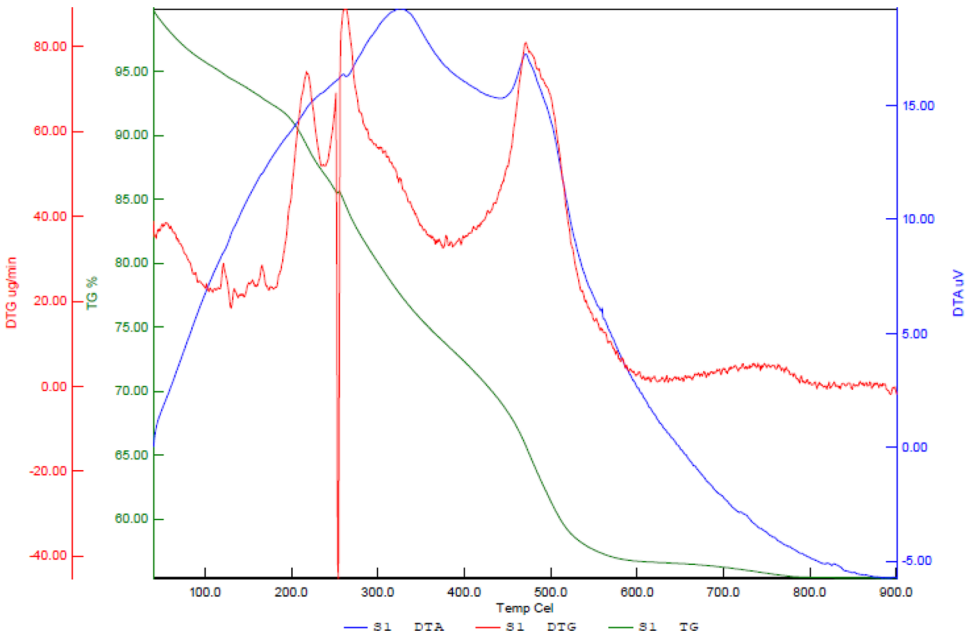

Fig. 7 DG-DTA curve of Ag-AI-NPs

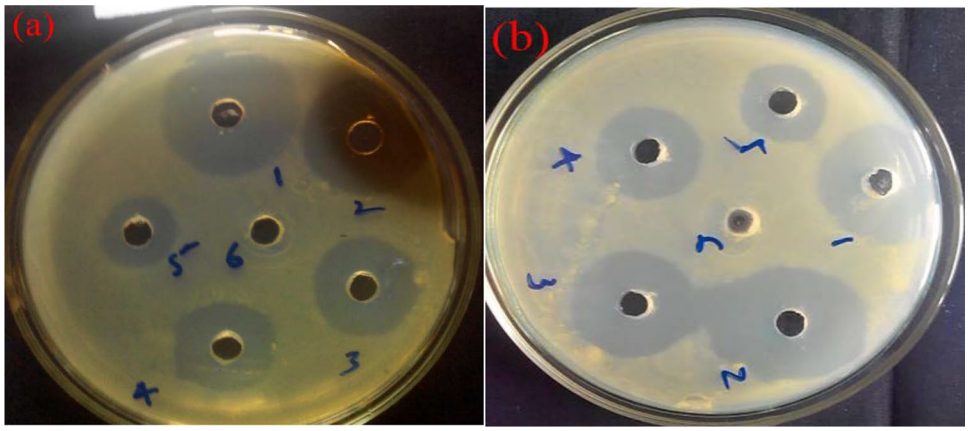

Fig. 8 **a** Antibacterial activity of Ag-AI-NPs against *P. aeruginosa*, and **b** *E. coli*

Table 2 Antibacterial efficacy of Ag-AI-NPs (ZOI in mm)

Ag-AI-NPs concentration						
Pathogen	1 mg/mL	500 µg/mL	250 µg/mL	125 µg/mL	62.5 µg/mL	Positive control (Ciproflaxacin-100 µg/mL)
P. aeruginosa	11.00 ± 0.000	9.00 ± 0.000	7.500 + 0.125	6.00 + 0.000	4.00 + 0.000	30.00 + 0.125
E. coli	15.50 + 0.250	13.00 + 0.125	10.00 + 0.825	8.500 + 0.000	6.00 + 0.000	35.25 + 0.125

of NPs responsible for capping and reduction of Ag ions to Ag NPs. The synthesized Ag-AI-NPs were found to be biocompatible and non-toxic retaining the cell viability of 83%. Green-synthesized NPs showed antibacterial activity but further research at molecular level has to be carried out to explore its potential for various biomedical applications.

Potential limitations of the study

The current study predominantly focuses on in vitro analysis of the antibacterial activity of Ag NPs. While in vitro studies provide initial insights, they may not fully replicate the complexities of living organisms. Additionally, the study does not include in vivo experiments to evaluate the cytotoxicity and overall biocompatibility of Ag NPs in living organisms. In vivo studies are crucial for understanding the actual biological interactions and potential side effects in a physiological context. The study may have tested a limited number of bacterial strains. Expanding the range of bacterial species, including resistant strains, could provide a more comprehensive understanding of the antibacterial efficacy of Ag NPs. Furthermore, the precise mechanism of the antibacterial action of Ag NPs is not fully elucidated in the study. Understanding the molecular pathways and targets involved would enhance the knowledge of how these NPs exert their effects. Lastly, the long-term toxicity and environmental impact of Ag NPs are not addressed. Assessing the ecological consequences and potential bioaccumulation is vital for the safe application of these NPs.

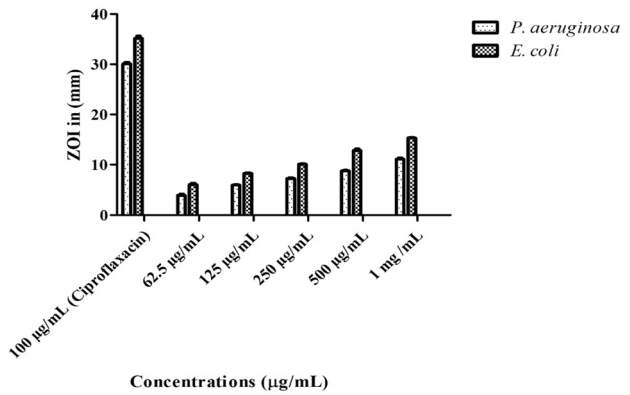

Fig. 9 Statistical significance of Ag-AI-NPs on test pathogens

Directions for future research

Future research should investigate the anticancer properties of Ag NPs. Given their biocompatibility, it is essential to evaluate their effectiveness against various cancer cell lines. This could involve studying the induction of apoptosis, inhibition of proliferation, and disruption of cancer cell signaling pathways. Conducting in vivo studies to assess the cytotoxicity and biocompatibility of Ag NPs is imperative. Animal models can be used to monitor biodistribution, clearance rates, organ-specific toxicity, and overall physiological impact. This will provide a clearer picture of the safety and potential therapeutic applications of Ag NPs. Detailed mechanistic studies are needed to elucidate the antibacterial and anticancer actions of Ag NPs. Techniques such as

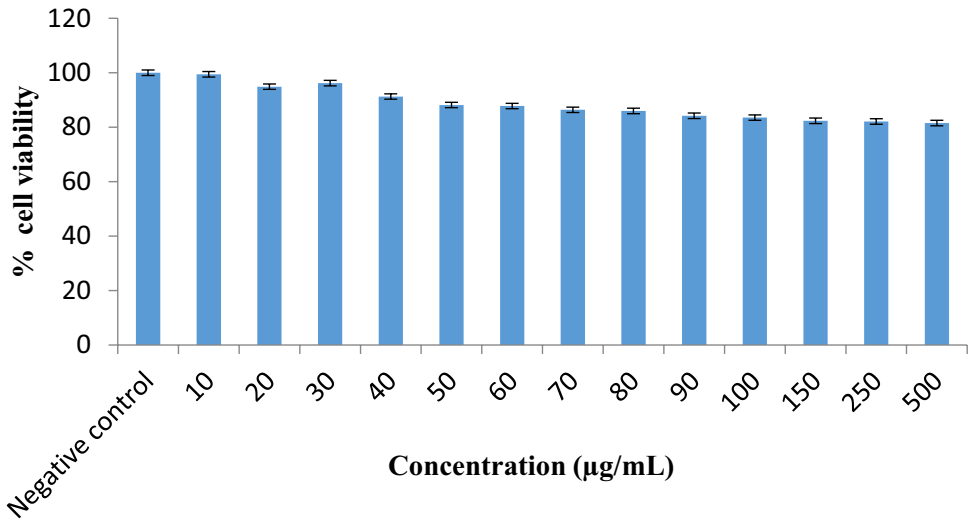

Fig. 10 MTT assay using L929 cell lines treated different concentration of Ag-NPs

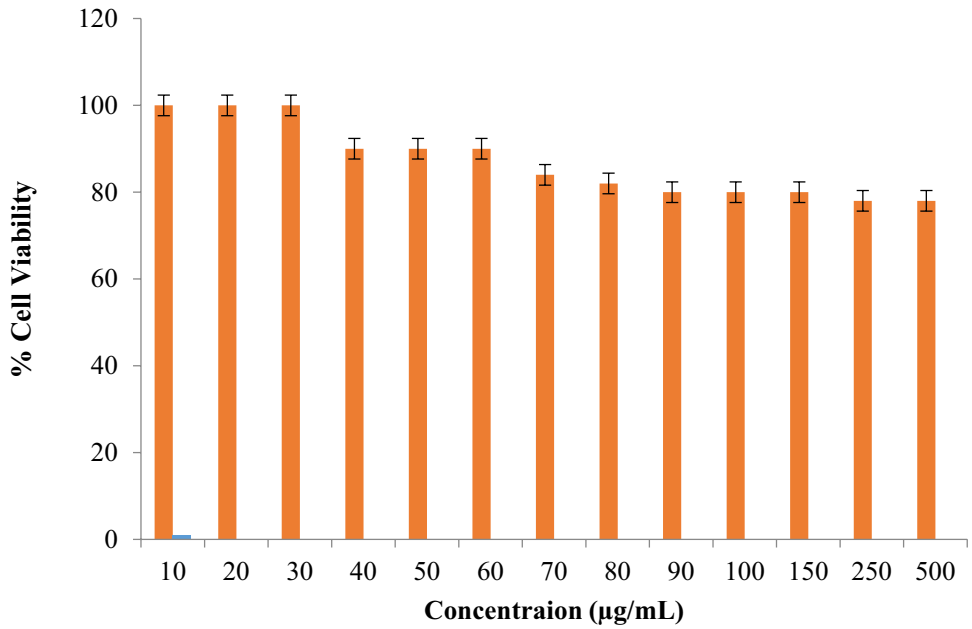

Fig. 11 MTT assay of ampicillin with $AgNO_3$

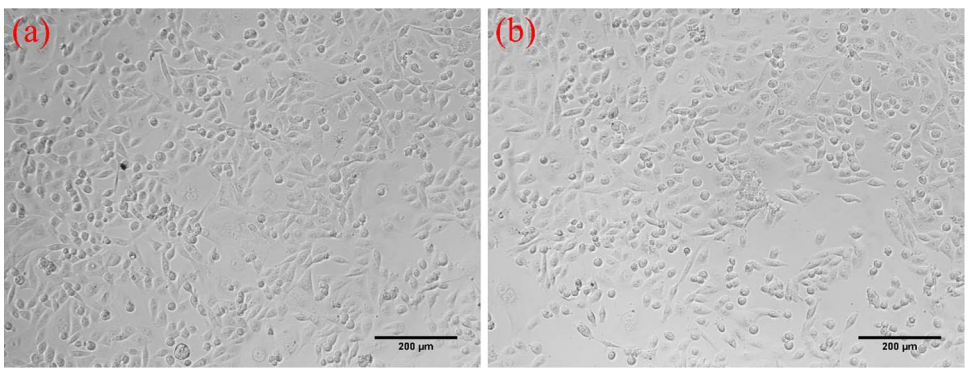

Fig. 12 L929 cells treated with **a** Ag–AI–NPs (500 µg/mL), and **b** $AgNO_3$ (500 µg/mL)

proteomics, genomics, and metabolomics could be employed to uncover the molecular targets and pathways involved. Investigating the synergistic effects of Ag NPs in combination with existing antibiotics or chemotherapeutic agents could offer new therapeutic strategies. Such combinatorial approaches might enhance efficacy and reduce the likelihood of resistance development. Assessing the long-term toxicity and environmental impact of Ag NPs is crucial. Studies should focus on their persistence in the environment, potential for bioaccumulation, and effects on non-target organisms. Developing guidelines for safe disposal and usage can mitigate environmental risks. Once preclinical studies demonstrate safety and efficacy, clinical trials should be conducted to evaluate the therapeutic potential of Ag NPs in human subjects. This includes determining optimal dosages, delivery methods, and monitoring for adverse effects.

Acknowledgements Authors are thankful to central instrument facility of Indian Institute of Technology, Guwahati, for carrying out transmission electron microscopy and field emission scanning electron microscopy.

Author contribution Conceptualization: Dr. Manoj Gadewar; Methodology, Investigation, Experimentation, Software, Data Interpretation: Dr. Manoj Gadewar, Dr. G.K. Prashanth; Draft Writing, Plagiarism Removal, Proofreading: Dr. Manoj Gadewar, Dr. G.K. Prashanth, Dr. Srilatha Rao, Dr. Lalithamba H.S., Dr. N.P. Bhagya, Dr. A.S. Sowyashree, Dr. K. Shwetha, Dr. Hemant Kumar N. Akolkar.

Funding None.

Data availability No data associated in the manuscript

Declarations

Conflict of interest The authors declare that they have no conflict of interest

Ethical approval Not required.

Consent to participate Not applicable.

Consent to publish Not applicable.

References

1. Minhas LA, Mumtaz AS, Kaleem M, Farraj DA, Kamal K, Minhas MAH, Mahmoud RM (2023) Green synthesis of zinc oxide nanoparticles using *Nostoc* sp. and their multiple biomedical properties. Catalysts 13(3):549
2. Minhas LA, Kaleem M, Minhas MAH, Waqar R, Al Farraj DA, Alsaigh MA, Mumtaz AS (2023) Biogenic fabrication of iron oxide nanoparticles from *Leptolyngbya* sp. L-2 and multiple in vitro pharmacogenetic properties. Toxics 11(7):561
3. Minhas LA, Kaleem M, Jabeen A, Ullah N, Farooqi HMU, Kamal A, Mumtaz AS (2023) Synthesis of silver oxide nanoparticles: a novel approach for antimicrobial properties and biomedical performance, featuring Nodularia Haraviana from the Cholistan desert. Microorganisms 11(10):2544
4. Malik HA, Minhas LA, Hassan MW, Kaleem M, Aslam F, Mumtaz AS (2024) Anabaena sp. A-1 mediated molybdenum oxide nanoparticles: a novel frontier in green synthesis, characterization and pharmaceutical properties. In: Microscopy research and technique. https://doi.org/10.1002/jemt.24572
5. Nagarajaiah S, Nanda N, Manjappa P, Nagabhushana BM, Gadewar M, Rao S, Krishna PG (2023) Evaluation of apoptosis in human breast cancer cell (MDA-MB-231) induced by ZnO nanoparticles synthesized using Piper betle leaf extract as bio-fuel. Appl Phys A 129(6):461
6. Prashanth GK, Sathyananda HM, Prashanth PA, Gadewar M, Muthuraju M, Prabhu SB, Mohanty D (2022) Controlled synthesis of Ag/CuO nanocomposites: evaluation of their antimycobacterial, antioxidant, and anticancer activities. Appl Phys A 128(7):614
7. Krishna PG, Ananthaswamy PP, Trivedi P, Chaturvedi V, Mutta NB, Sannaiah A, Erra A, Yadavalli T (2017) Antitubercular activity of ZnO nanoparticles prepared by solution combustion synthesis using lemon juice as bio-fuel. Mater Sci Eng C 75:1026–1033
8. Prashanth GK, Prashanth PA, Bora U, Gadewar M, Nagabhushana BM, Ananda S, Krishnaiah GM, Sathyananda HM (2015) In vitro antibacterial and cytotoxicity studies of ZnO nanopowders prepared by combustion assisted facile green synthesis. Karbala Int J Mod Sci 1(2):67–77
9. Yazdi M, Yousefvand A, Hosseini HM, Mirhosseini SA (2022) Green synthesis of silver nanoparticles using Nisin and its antibacterial activity against *Pseudomonas aeruginosa*. Adv Biomed Res 11:56. https://doi.org/10.4103/abr.abr_99_21
10. Boisselier E, Astruc D (2009) Gold nanoparticles in nanomedicine: preparations, imaging, diagnostics, therapies and toxicity. Chem Soc Rev 38:1759–1782. https://doi.org/10.1039/b806051g
11. Mousavi-Kouhi SM, Beyk-Khormizi A, Amiri MS, Mashreghi M, Yazdi MET (2021) Silver-zinc oxide nanocomposite: from synthesis to antimicrobial and anticancer properties. Ceramics Int 47(15):21490–21497
12. Sathyananda HM, Prashanth PA, Prashanth GK, Nagabhushana BM, Krishnaiah GM, Nagendra HG, Dileep MS, Ananda S, Boselin Prabhu SR (2021) Evaluation of antimicrobial, antioxidant, and cytotoxicity activities of CuO nanopellets synthesized by surfactant-free hydrothermal method. J Test Eval 49(6):4170–4180
13. Suresh P, Doss A, Praveen Pole RP, Devika M (2024) Green synthesis, characterization and antioxidant activity of bimetallic (Ag-ZnO) nanoparticles using Capparis zeylanica leaf extract. Biomass Conversion and Biorefinery 14(14):16451–16459
14. Rahimi E, Asefi F, Afzalinia A, Khezri S, Zare-Zardini H, Ghorani-Azam A, Es-haghi A, Yazdi MET (2023) Chitosan coated copper/silver oxide nanoparticles as carriers of breast anticancer drug: cyclin D1/P53 expressions and cytotoxicity studies. Inorg Chem Commun 158:111581
15. De Jong WH, Borm PJA (2008) Drug delivery and nanoparticles: applications and hazards. Int J Nanomed 3:133–149. https://doi.org/10.2147/ijn.s596
16. Yin IX, Zhang J, Zhao IS, Mei ML, Li Q, Chu CH (2020) The antibacterial mechanism of silver nanoparticles and its application in dentistry. Int J Nanomed 15:2555–2562. https://doi.org/10.2147/IJN.S246764
17. Pem B, Pongrac IM, Ulm L, Pavičić I, Vrček V, Domazet Jurašin D, Ljubojević M, Krivohlavek A, Vinković Vrček I (2019) Toxicity and safety study of silver and gold nanoparticles functionalized with cysteine and glutathione. Beilstein J Nanotechnol 10:1802–1817. https://doi.org/10.3762/bjnano.10.175
18. Kim M, Osone S, Kim T, Higashi H, Seto T (2017) Synthesis of nanoparticles by laser ablation: a review. KONA Powder Part J 34:80–90

19. El-Eskandarany MS, Al-Hazza A, Al-Hajji LA, Ali N, Al-Duweesh AA, Banyan M, Al-Ajmi F (2021) Mechanical milling: a superior nanotechnological tool for fabrication of nanocrystalline and nanocomposite materials. Nanomater. https://doi.org/10.3390/nano11102484
20. Cheng W, Zhang W, Hu L, Ding W, Wu F, Li J (2016) Etching synthesis of iron oxide nanoparticles for adsorption of arsenic from water. Rsc Adv 6:15900–15910
21. Sobolev A, Musin A, Whyman G, Borodianskiy K, Krichevski O, Kalashnikov A, Zinigrad M (2019) Stabilization of cubic phase in scandium-doped zirconia nanocrystals synthesized with sol–gel method. J Am Ceram Soc 102:3236–3243
22. Türk M, Erkey C (2018) Synthesis of supported nanoparticles in supercritical fluids by supercritical fluid reactive deposition: current state, further perspectives and needs. J Supercrit Fluids 134:176–183
23. Sourice J, Quinsac A, Leconte Y, Sublemontier O, Porcher W, Haon C, Bordes A, Vito E, Boulineau A, Jouanneau Si Larbi S, Herlin-Boime N (2015) One-step synthesis of Si@ C nanoparticles by laser pyrolysis High-capacity anode material for lithium-ion batteries. ACS appl mater Interfaces 7(12):6637–6644
24. Hussain MH, Abu Bakar NF, Mustapa AN, Low K-F, Othman NH, Adam F (2020) Synthesis of various size gold nanoparticles by chemical reduction method with different solvent polarity. Nanoscale Res Lett 15:140. https://doi.org/10.1186/s11671-020-03370-5
25. Bindhu MR, Umadevi M, Esmail GA, Al-Dhabi NA, Arasu MV (2020) Green synthesis and characterization of silver nanoparticles from *Moringa oleifera* flower and assessment of antimicrobial and sensing properties. J Photochem Photobiol B 205:111836. https://doi.org/10.1016/j.jphotobiol.2020.111836
26. Ying S, Guan Z, Ofoegbu PC, Clubb P, Rico C, He F, Hong J (2022) Green synthesis of nanoparticles: current developments and limitations. Environ Technol Innov 26:102336
27. Messaoudi El, Noureddine ZC, Şenol ZM, Kazan-Kaya ES, Fernine Y, Gubernat S, Lopicic Z (2024) Green synthesis of $CuFe_2O_4$ nanoparticles from bioresource extracts and their applications in different areas: a review. Biomass Convers Biorefinery. https://doi.org/10.1007/s13399-023-05264-9
28. Mousavi SM, Hashemi SA, Ghasemi Y, Atapour A, Amani AM, Savar Dashtaki A, Babapoor O (2018) Green synthesis of silver nanoparticles toward bio and medical applications: review study. Artif Cells Nanomed Biotechnol 46:S855–S872. https://doi.org/10.1080/21691401.2018.1517769
29. Yin M, Xu X, Han H, Dai J, Sun R, Yang L, Xie J, Wang Y (2022) Preparation of triangular silver nanoparticles and their biological effects in the treatment of ovarian cancer. J Ovarian Res 15:121
30. Shashiraj KN, Hugar A, Kumar RS, Rudrappa M, Bhat MP, Almansour AI, Nayaka S (2023) Exploring the antimicrobial, anticancer, and apoptosis inducing ability of biofabricated silver nanoparticles using *Lagerstroemia speciosa* flower buds against the human osteosarcoma (MG-63) cell line via flow cytometry. Bioengineering 10(7):821
31. Math HH, Shashiraj KN, Kumar RS, Rudrappa M, Bhat MP, Basavarajappa DS, Nayaka S (2023) Investigation of in vitro anticancer and apoptotic potential of biofabricated silver nanoparticles from *Cardamine hirsuta* (L.) leaf extract against Caco-2 cell line. Inorganics 11(8):322
32. Sangeeta MK, Tejashree VM, Gunagambhire MPB, Nagaraja SK, Gunagambhire PV, Suresh Kumar R, Mahalingam SM (2024) In-vitro evaluation of Talaromyces Islandicus mediated zinc oxide nanoparticles for antibacterial, anti-inflammatory, bio-pesticidal and seed growth promoting activities. Waste Biomass Valor 15(3):1901-1915
33. Bhat M, Chakraborty B, Kumar RS, Almansour AI, Arumugam N, Kotresha D, Pallavi SS, Dhanyakumara SB, Shashiraj KN, Nayaka S (2021) Biogenic synthesis, characterization and antimicrobial activity of Ixora brachypoda (DC) leaf extract mediated silver nanoparticles. J King Saud Univ-Sci (2):101296
34. Rudrappa M, Rudayni HA, Assiri RA, Bepari A, Basavarajappa DS, Nagaraja SK, Chakraborty B, Swamy PS, Agadi SN, Niazi SKm Nayaka S (2022) Plumeria alba-mediated green synthesis of silver nanoparticles exhibits antimicrobial effect and anti-oncogenic activity against glioblastoma U118 MG cancer cell line. Nanomaterials 12(3):493
35. Nagarajaiah S, Shivanna Giresha A, Gopala Krishna P, Manikrao Gadewar M, Praveen M, Nanda N, Urs D, Krishnappa Dharmappa K, Mutta Nagabhushana B, Rao S, Mahadeva Swamy M (2024) Anti-oncogenic potential and inflammation modulatory response of green synthesized biocompatible silver nanoparticles. Chem Biodiver 21(3):e202301533
36. Kazemi M, Dakhili M, Dadkhah A, Fadaeian M, Shafizadeh S (2013) Composition, antimicrobial and antioxidant activities of Artemisia deserti Kracsh essential oil from Iran. Asian J Chem 25:47
37. Nahid A, Neelabh C, Navneet K (2017) Antioxidant and antimicrobial potentials of *Artemisia Indica* collected from the Nepal region. J Pharm Sci Res 9:1822–1826
38. Tasdemir D, Tierney M, Sen R, Bergonzi MC, Demirci B, Bilia AR, Baser KHC, Brun R, Chatterjee M (2015) Antiprotozoal effect of *Artemisia Indica* extracts and essential oil. Planta Med 81:1029–1037
39. Chanphen R, Thebtaranonth Y, Wanauppathamkul S, Yuthavong Y (1998) Antimalarial principles from *Artemisia Indica*. J Nat Prod 61:1146–1147. https://doi.org/10.1021/np980041x
40. Tiwary BK, Bihani S, Kumar A, Chakraborty R, Ghosh R (2015) The in vitro cytotoxic activity of ethno-pharmacological important plants of Darjeeling district of West Bengal against different human cancer cell lines. BMC Complement Altern Med 15:22. https://doi.org/10.1186/s12906-015-0543-5
41. Khan I, Karim N, Ahmad W, Abdelhalim A, Chebib M (2016) GABA-A receptor modulation and anticonvulsant, anxiolytic, and antidepressant activities of constituents from *Artemisia Indica* Linn. Evid Based Complement Alternat Med 2016:1215393. https://doi.org/10.1155/2016/1215393
42. Khan I, Ahmad W, Karim N, Ahmad M, Khan M, Tariq SA, Sultana N, Shah R, Khan A, Abdelhalim A (2017) Antidiabetic activity and histopathological analysis of carnosol isolated from *Artemisia Indica* linn in streptozotocin-induced diabetic rats. Med Chem Res 26:335–343
43. Sagar MK, Ashok PK, Chopra H, Upadhyaya K (2010) Phytochemical and pharmacological potential of *Artemisia Indica* in experimental animal models. Pharmacologyonline 2:1–4
44. Khan S, Afshan K, Mirza B, Miller JE, Manan A, Irum S, Rizvi SSR, Qayyum M (2015) Anthelmintic properties of extracts from Artemisia plants. Trop Biomed 32:257–268
45. Nadeem M, Tungmunnithum D, Hano C, Abbasi BH, Hashmi SS, Ahmad W, Zahir A (2018) The current trends in the green syntheses of titanium oxide nanoparticles and their applications. Green Chem Lett Rev 11:492–502. https://doi.org/10.1080/17518253.2018.1538430
46. Jadoun S, Arif R, Jangid NK, Meena RK (2021) Green synthesis of nanoparticles using plant extracts: a review. Env Chem Lett 19:355–374. https://doi.org/10.1007/s10311-020-01074-x
47. Gadewar M et al (2023) Unlocking nature's potential: green synthesis of ZnO nanoparticles and their multifaceted applications-a concise overview. J Saudi Chem Soc 28(1):101774
48. Njema GG, Ouma RB, Kibet JK (2024) A review on the recent advances in battery development and energy storage technologies. J Renew Energy 2024(1):2329261

49. Sathyananda HM, Prashanth PA, Prashanth GK, Dileep MS, Boselin Prabhu SR, Nagabhushana BM, Shivakumara C, Nagendra HG (2022) Evaluation of antimycobacterial, antioxidant, and anticancer activities of CuO nanoparticles through cobalt doping. Appl Nanosci 12:79–86
50. Prashanth GK, Prashanth PA, Ramani M, Ananda S, Nagabhushana BM, Krishnaiah GM, Nagendra HG, Sathyananda HM, Mutthuraju M, Rajendra Singh C (2019) Comparison of Antimicrobial, Antioxidant and Anticancer Activities of ZNPs Nanoparticles Prepared by Lemon Juice and Citric Acid Fueled Solution Combustion Synthesis. Bionanoscience 9:799–812 https://doi.org/10.1007/s12668-019-00670-8
51. P GK, Prashanth PA, Singh P, Nagabhushana BM, Shivakumara C, K GM, Nagendra HG, Sathyananda HM, Chaturvedi V (2020) Effect of Doping (with Cobalt or Nickel) and UV exposure on the antibacterial, anticancer, and ROS generation activities of zinc oxide nanoparticles. J asian Ceram Soc 8:1175–1187
52. Meti RS, Neelagund SE, Urs D et al (2023) Green synthesis of silver nanoparticles from *Acacia sinuata* seed extract and evaluation of their mosquitocidal and anticancer (Caco-2 and MG-63 cell) activity. Biomass Conv Bioref. https://doi.org/10.1007/s13399-023-05161-1
53. Sánchez-Moreno C (2002) Food Sci Technol Int 8:121–137
54. Chang CC, Yang MH, Wen HM, Chern JC (2002) J Food Drug Anal 10:178–182
55. Castillo-Henríquez L, Alfaro-Aguilar K, Ugalde-Álvarez J, Vega-Fernández L, Montes de Oca-Vásquez G, Vega-Baudrit JR (2020) Green synthesis of gold and silver nanoparticles from plant extracts and their possible applications as antimicrobial agents in the agricultural area. Nanomater. https://doi.org/10.3390/nano10091763
56. Kemboi D, Langat MK, Siwe-Noundou X, Krause RWM, Isaacs ML, Tembu VJ (2022) In vitro antibacterial and cytotoxic effects of Euphorbia grandicornis Blanc chemical constituents. BMC Complement Med Ther 22:90. https://doi.org/10.1186/s12906-022-03571-8
57. Kumar SV, Bafana AP, Pawar P, Rahman A, Dahoumane SA, Jeffryes CS (2018) High conversion synthesis of< 10 nm starch-stabilized silver nanoparticles using microwave technology. Sci Rep 8:5106
58. Shashiraj KN, Nayaka S, Kumar RS, Kantli GB, Basavarajappa DS, Gunagambhire PV, Almansour AI, Perumal K (2023) *Rotheca serrata* flower bud extract mediated bio-friendly preparation of silver nanoparticles: their characterizations, anticancer, and apoptosis inducing ability against pancreatic ductal adenocarcinoma cell line. Processes 11(3):893. https://doi.org/10.3390/pr11030893
59. Nagaraja SK, Kumar RS, Chakraborty B et al (2023) Biomimetic synthesis of silver nanoparticles using *Cucumis sativus* var. *hardwickii fruit* extract and their characterizations, anticancer potential and apoptosis studies against Pa-1 (Human ovarian teratocarcinoma) cell line via flow cytometry. Appl Nanosci 13:3073–3084. https://doi.org/10.1007/s13204-022-02386-w
60. Nagaraja SK, Niazi SK, Bepari A, Assiri RA, Nayaka S (2022) *Leonotis nepetifolia* flower bud extract mediated green synthesis of silver nanoparticles, their characterization, and in vitro evaluation of biological applications. Materials 15(24):8990. https://doi.org/10.3390/ma15248990
61. Basavarajappa DS, Kumar RS, Almansour AI, Chakraborty B, Bhat MP, Nagaraja SK, Nayaka S (2022) Biofunctionalized silver nanoparticles synthesized from Passiflora vitifolia leaf extract and evaluation of its antimicrobial, antioxidant and anticancer activities. Biochem Eng J 187:108517
62. Harish V, Tewari D, Mohd S, Govindaiah P, Babu MR, Kumar R, Gulati M, Gowthamarajan K, Madhunapantula SV, Chellappan DK, Gupta G, Dua K, Dallavalasa S, Singh SK (2022) Quality by design based formulation of Xanthohumol loaded solid lipid nanoparticles with improved bioavailability and anticancer effect against PC-3 cells. Pharmaceutics 14:2403. https://doi.org/10.3390/PHARMACEUTICS14112403
63. Arif M, Ullah R, Ahmad M, Ali A, Ullah Z, Ali M, Al-Joufi FA, Zahoor M, Sher H (2022) Green synthesis of silver nanoparticles using *Euphorbia wallichii* leaf extract: its antibacterial action against citrus canker causal agent and antioxidant potential. Molecules. https://doi.org/10.3390/MOLECULES27113525
64. Srinivasan D, Nathan S, Suresh T, Perumalsamy PL (2001) Antimicrobial activity of certain Indian medicinal plants used in folkloric medicine. J Ethnopharmacol 74:217–220
65. Gonzalez RJ, Tarloff JB (2001) Evaluation of hepatic subcellular fractions for Alamar blue and MTT reductase activity. Toxicol Vitr 15:257–259
66. Lu GW, Gao P (2010) Emulsions and microemulsions for topical and transdermal drug delivery. In: Handbook of non-invasive drug delivery systems. William Andrew Publishing, pp. 59–94. https://doi.org/10.1016/B978-0-8155-2025-2.10003-4
67. Buazar F, Bavi M, Kroushawi F, Halvani M, Khaledi-Nasab A, Hossieni SA (2016) Potato extract as reducing agent and stabiliser in a facile green one-step synthesis of ZnO nanoparticles. J Exp Nanosci 11:175–184
68. Kim JS, Kuk E, Yu KN, Kim J-H, Park SJ, Lee HJ, Kim SH, Park YK, Park YH, Hwang C-Y (2007) Antimicrobial effects of silver nanoparticles, nanomedicine nanotechnology. Biol Med 3:95–101
69. Whibley CE, McPhail KL, Keyzers RA, Maritz MF, Leaner VD, Birrer MJ et al (2007) Mol Cancer Ther 6(9):2535–2543
70. Ravid A, Koren R (2003) Recent Results Cancer Res 164:357–367
71. Marambio-Jones C, Hoek EMV (2010) J Nanopart Res 12:1531–1551
72. Mukherjee S, Chowdhury D, Kotcherlakota R, Patra S, Vinothkumar B, Bhadra MP, Sreedhar B, Patra CR (2014) Potential theranostics application of bio-synthesized silver nanoparticles (4-in-1 system). Theranostics 4(3):316